INFLUENCE OF MICRO-CRACKING ON THE EFFECTIVE PROPERTIES OF COMPOSITE MATERIALS

Domenico Bruno, Fabrizio Greco, Paolo Lonetti, Paolo Nevone Blasi

University of Calabria, Department of Structural Engineering,
87036 Arcavacata di Rende (CS), Italy

d.bruno@unical.it (Domenico Bruno)

Abstract

In the present work the influence of micro-cracking on the effective properties of composite materials with heterogenous micro-structure is investigated by using the finite element method in conjunction with interface models. Non-linear macroscopic constitutive laws are developed by taking into account for changes in micro-structural configuration associated with the growth of micro-cracks. Damage evolution is simulated by micro-mechanical considerations using fracture mechanics. The strong non-linearity of the macroscopic constitutive response results in a progressive loss of stiffness and may lead to failure for homogeneous macro-deformations associated with unstable crack propagation. Both the cases of a brittle matrix composite with micro-cavities and of a fiber-reinforced composite with imperfect interfacial bonding are considered, loaded along extension and compression uniaxial macro-strain paths. In the context of deformation controlled micro-structures, three types of boundary conditions are studied, namely linear deformation, uniform tractions and periodic deformations and antiperiodic tractions. These conditions, which can be incorporated by means of Lagrangian multiplier methods, generate three constrained minimization problems of homogenization which define the micro-to-macro transition and determine the state of the micro-structure in terms of the fine-scale fluctuation field. Micro-crack propagation is modeled by using the *J*-integral methodology in conjunction with an interface model taking into account for contact between crack faces. The proposed damage model is able to provide constitutive laws for the microstructure with evolving defects and may provide a failure model for a composite material undergoing micro-cracking and contact.

Keywords: Micro-cracks and interfacial debonding, Macroscopic properties, Composite material, Contact, Finite elements

Presenting Author's biography

Fabrizio Greco. Born in Catanzaro (Italy) the 2nd September 1973. *Position*: from January 2005 Associate Professor of Structural Engineering at the Department of Structural Engineering of University of Calabria. *Teaching Activities*: Statics, Dynamics of Structures, Strength of materials. *Current research activities*: Composite materials, Damage, Fracture, Stability, Homogenization, Long span bridges.

1 Introduction

The prediction of the macroscopic constitutive properties of various composite materials by taking into account for their microscopic behavior, is a problem of great importance due to the increasing application of composites to practical structures. Recognizing explicitly the micro-structure of a composite material in the mathematical model, by distinguishing the individual phases of a composite material, such as the fiber, matrix and interphases, requires a large numerical effort. Therefore several approaches have been proposed for obtaining the macroscopic response of a heterogeneous material. In addition to analytical methods [1,2], two basic methodologies can be adopted which can be classified into the average-field method and the homogenization method. The former approach is based on the physical evidence that the mechanical properties measured during experiments are relations between volume averages of microscopically heterogeneous samples (see for instance [3,4]). The latter approach formulates the relations between micro- and macro-variables on the basis of the mathematical procedure of multi-scale perturbation assuming a periodic model for the microstructure (see for example [5,6]). As shown in ([7]) these two methods may produce the same overall properties when the homogenization theory is formulated in a specialized setting, and are often applied in conjunction with FEM.

In many cases damage phenomena may occur at the microscopic level, such as void growth, micro-cracking, imperfect bond between different phases. These damage mechanisms affect seriously the macroscopic behavior of the composite material. As a matter of fact, even if each individual phase follows a linear elastic constitutive behavior, the changes in the microstructure due to the evolving damage mechanisms, give raise to a strongly non-linear macroscopic constitutive relationship. The non-linearity of the macroscopic constitutive response results in a progressive loss of stiffness and may lead to failure for homogeneous macro-deformations associated with unstable crack propagation (a peak stress). A realistic micromechanical model should give a constitutive law at the macro-level able to represent with reasonable accuracy material failure mechanisms.

Many studies have been devoted on the effective constitutive behavior of defected composites, with reference to both fiber composite materials with fiber-matrix interfacial debonding (see [8-12] for instance) and materials containing voids and microcracks (see for instance [13-15]). Since damage in a composite material is a non-linear process, the determination of stiffness properties evolution with progressive damage is a complex but necessary task. Since for a pure micromechanical model the evolving configuration of damage cannot be predicted, many authors have assumed arbitrarily the configuration of damage [8, 9, 10]. More general approaches are to consider a random distribution of interface cracks or debonding [11], to include damage evolution effects into the macroscopic constitutive law by means of brittle interface models [12], or by incorporating fracture mechanics based damage evolution law [14].

In this work the influence of micro-cracking on the effective properties of composite materials with heterogeneous micro-structure is investigated by using the finite element method in conjunction with interface models. Non-linear macroscopic constitutive laws are developed by taking into account for the progressive changes in micro-structural configuration associated with the growth of micro-cracks. Damage evolution is simulated by micro-mechanical considerations using fracture mechanics. Both the cases of a brittle matrix composite with micro-cavities and of a fiber-reinforced composite with imperfect interfacial bonding are considered. Three classes of boundary conditions are studied, namely linear deformation, uniform tractions and periodic deformation and antiperiodic traction, in the framework of deformation controlled micro-structures. Micro-crack propagation is simulated by means of the *J*-integral methodology in coupling with an interface model taking into account for unilateral frictionless contact between crack faces. Results show that, besides on the geometries and the properties of the individual components which form the representative micro-structure of the composite material, the macroscopic constitutive law depends on the macro-strain path and the type of boundary conditions.

2 Formulation

2.1 Basic equations

A representative volume, $V=S\cup H$, of the composite micro-structure is considered in Fig. 1, which consists of a solid part S and a hole part H, including microscopic discontinuities (cracks and interface debonding) and/or cavities. The representative volume may contain an arbitrary number of individual phases imperfectly bonded, micro-cracks and micro-voids. The boundary of the hole part ∂H represents the union of micro-crack, including interface crack, and micro-void surfaces. Let $\boldsymbol{u}(\boldsymbol{x})$ denotes the displacement field of the micro-structure at the material point $\boldsymbol{x}$, and $\boldsymbol{\varepsilon}(\boldsymbol{u}(\boldsymbol{x}))$ the associated microscopic strain field. The micro-structure is loaded by tractions only on the surface ∂V of the representative volume. The microscopic traction field $\boldsymbol{t}$ is assumed to vanish on the surfaces of the holes and cracks in the interior of the representative volume, namely $\boldsymbol{t}=\boldsymbol{0}$ on ∂H. Due to the large scale difference between the microscopic problem and the macroscopic one, according to the classical homogenization theory the macroscopic constitutive response of the micro-structure is based on a equilibrium state neglecting volume forces,

implying that the local stress field $\boldsymbol{\sigma}$ is divergence-free, namely Div($\boldsymbol{\sigma}$)=$\boldsymbol{0}$ in S.

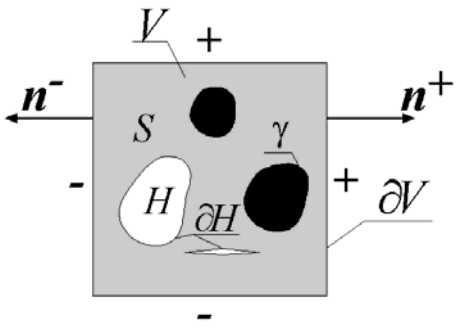

Fig. 1 Representative volume element of a heterogeneous micro-structure containing micro-cavities, micro-cracks and inclusions.

The macroscopic stress and strain fields are defined in terms of boundary data of tractions $\boldsymbol{t}$ and displacements $\boldsymbol{u}$ [16] respectively as

$$\bar{\boldsymbol{\sigma}} = \frac{1}{|V|}\int_{\partial V} \boldsymbol{t}\otimes\boldsymbol{x}dA, \quad \bar{\boldsymbol{\varepsilon}} = \frac{1}{|V|}\int_{\partial V} \boldsymbol{u}\otimes_s \boldsymbol{n}dA\,, \tag{1}$$

where $\otimes_s$ is the symmetric part the tensor product $\otimes$ and $\boldsymbol{n}$ denotes the outward normal at $\boldsymbol{x}\in\partial S$. The above definition of macro-variables coincides with the volume average over V for the macroscopic stress and only for micro-structures without holes and discontinuities for the macroscopic strain. As a matter of fact, application of the integral theorem gives the expression:

$$\begin{aligned}\bar{\boldsymbol{\sigma}} &= \frac{1}{|V|}\int_V \boldsymbol{\sigma}dV,\\ \bar{\boldsymbol{\varepsilon}} &= \frac{1}{|V|}\int_V \boldsymbol{\varepsilon}dV - \frac{1}{|V|}\int_{\partial H} \boldsymbol{u}\otimes_s \boldsymbol{n}dA\end{aligned}. \tag{2}$$

Note that in Eq. (2) the term on the boundary $-1/|V|\int_{\partial H}\boldsymbol{t}\otimes\boldsymbol{x}dA$ vanishes since the hole is assumed traction free and in presence of frictionless contact continuity of the traction vector is ensured across the crack surfaces undergoing into contact. The local displacement field is assumed to be controlled by a macroscopic strain $\bar{\boldsymbol{\varepsilon}}$, and consists of a linear part $\bar{\boldsymbol{\varepsilon}}\boldsymbol{x}$ and a fluctuation field $\boldsymbol{w}$. The microscopic displacement and strain field therefore admit the following representation:

$$\boldsymbol{u}(\boldsymbol{x})=\bar{\boldsymbol{\varepsilon}}\boldsymbol{x}+\boldsymbol{w}(\boldsymbol{x}), \quad \boldsymbol{\varepsilon}(\boldsymbol{x}) = \bar{\boldsymbol{\varepsilon}}+\nabla_s\boldsymbol{w}\,, \tag{3}$$

where ∇_s denotes the symmetric part of the gradient with respect to $\boldsymbol{x}$. As a consequence of Eq. (1), the fluctuation field must satisfy the constraint:

$$\frac{1}{|V|}\int_{\partial V} \boldsymbol{w}\otimes_s \boldsymbol{n}dA = \boldsymbol{0}\,, \tag{4}$$

which can be satisfied for three alternative boundary conditions on ∂V (see [17] for instance):

1) homogeneous fluctuations $\boldsymbol{w}=\boldsymbol{0}$;

2) periodic fluctuations $\boldsymbol{w}(\boldsymbol{x}^+)=\boldsymbol{w}(\boldsymbol{x}^-)$; (5)

3) homogeneous stress $\boldsymbol{t}=\bar{\boldsymbol{\sigma}}\boldsymbol{n}$;

where by periodicity of the field $\boldsymbol{w}(\boldsymbol{x})$ it is assumed that all components of $\boldsymbol{w}(\boldsymbol{x})$ take identical values at points on opposite sides of the boundary ∂V, ∂V^+ and ∂V^-, with outwards normals $\boldsymbol{n}^+=-\boldsymbol{n}^-$ at two associated points $\boldsymbol{x}^+\in\partial V^+$ and $\boldsymbol{x}^-\in\partial V^-$, which are deduced by translation parallel to the directions of the vectors spanning V. In the third condition, Eq. (4) is intended to be satisfied in a global sense, since the macro-stress is not a-priori known but it is understood to be calculated for a given macro-strain $\bar{\boldsymbol{\varepsilon}}$ by treating Eq. $(1)_2$ as the following weak constraint:

$$\bar{\boldsymbol{\sigma}}\bullet\bar{\boldsymbol{\varepsilon}}-\frac{1}{|V|}\int_{\partial V}\bar{\boldsymbol{\sigma}}\bullet\left(\boldsymbol{u}\otimes_s\boldsymbol{n}\right)dA = 0\,, \tag{6}$$

where the macro-stress tensor acts as a Lagrange multiplier. By assuming the anti-periodicity of the tractions on ∂V, these boundary conditions satisfy the averaging theorem ([16]):

$$\bar{\boldsymbol{\sigma}}\bullet\bar{\boldsymbol{\varepsilon}}=\frac{1}{|V|}\int_S \sigma\bullet\varepsilon dV = \frac{1}{|V|}\int_{\partial V}\boldsymbol{t}\bullet\boldsymbol{u}dA\,, \tag{7}$$

which plays a central role in the definition of macroscopic properties of the composite material. It is worth noting that the first and third of boundary conditions (5) provide upper and lower strain energy bounds for representative volume elements (RVEs) of irregular materials with a finite size, which converge to a common value as the size of the RVE becomes infinitely large. On the other hand the second one yields exact results for a unit-cell of periodic materials, which generates by periodic repetition the whole micro-structure of the composite.

The local constitutive response of the composite material is assumed linearly hyperelastic with tensor of microscopic moduli $\boldsymbol{C}(\boldsymbol{x})$. The homogenization condition can be obtained by means of the following minimization problem:

$$\bar{W}\left(\bar{\boldsymbol{\varepsilon}}\right) = \inf_{\boldsymbol{w}\in A(\bar{\boldsymbol{\varepsilon}})}\frac{1}{|V|}\int_V W\left(\boldsymbol{\varepsilon}(\boldsymbol{u}),\boldsymbol{x}\right)dV\,, \tag{8}$$

subjected to the above mentioned three alternative constraints, providing the macro-stress potential as the minimum volume average of the microscopic strain energy W with respect to admissible fluctuation fields $A(\bar{\boldsymbol{\varepsilon}})$ alternatively satisfying the constraints $(5)_1$, $(5)_2$ and $(5)_3$. From (8) and (7), it follows that the macro-stress potential defines the macro-stress and moduli in terms of the first and second derivatives of the macro-stress potential with respect to the macro-strain:

$$\bar{\boldsymbol{\sigma}} = \frac{\partial \bar{W}}{\partial \bar{\boldsymbol{\varepsilon}}}, \quad \bar{\boldsymbol{C}} = \frac{\partial^2 \bar{W}}{\partial \bar{\boldsymbol{\varepsilon}}^2}. \tag{9}$$

When the local problem (8) is linear, it follows that

$$\bar{\boldsymbol{\sigma}} = \frac{1}{|V|}\int_V \boldsymbol{C}(\boldsymbol{x})\boldsymbol{\varepsilon}(\boldsymbol{u})\,dV = \bar{\boldsymbol{C}}\bar{\boldsymbol{\varepsilon}}$$
$$\bar{\boldsymbol{C}}_{ijhk} = \frac{1}{|V|}\int_V \boldsymbol{C}_{ijmn}(\boldsymbol{x})\boldsymbol{\varepsilon}_{mn}(\boldsymbol{u}^{hk})\,dV = \frac{1}{|V|}\int_V \boldsymbol{C}(\boldsymbol{x})\boldsymbol{\varepsilon}(\boldsymbol{u}^{hk})\bullet\boldsymbol{\varepsilon}(\boldsymbol{u}^{ij})\,dV \tag{10}$$

where $\boldsymbol{u}^{ij}$ is the solution of (8) for a unit prescribed macro-strain $\bar{\boldsymbol{\varepsilon}}^{ij} = \boldsymbol{e}_i \otimes_s \boldsymbol{e}_j$ with $\boldsymbol{e}_i$ unit vectors parallel to the coordinate axes x_i. Note that the macro-moduli tensor $(10)_2$ satisfy the diagonal symmetry as a consequence of the assumed hyperelasticity of micro-constituents. On the other hand, when unilateral frictionless contact conditions are taken into account at the debonded interfaces or micro-cracks surfaces, the variational principle (8) can be generalized by appropriate choose of the admissible strain field (see [9] for instance) and the macroscopic constitutive behavior of the composite turns out to be nonlinear but remains hyperelastic (rate- and path- independent). As a matter of fact, the contact area is not a-priori known and depends on the direction of the prescribed macro-strain, and this implies that the tensor of macroscopic moduli $\bar{\boldsymbol{C}} = \bar{\boldsymbol{C}}(\bar{\varepsilon})$ (Eq. $(9)_2$ is here intended as second Gateaux derivative when it exists) satisfies $\bar{\boldsymbol{C}}(\lambda\bar{\varepsilon}) = \bar{\boldsymbol{C}}(\bar{\varepsilon})$ for every positive real λ. On the other hand, the macro-stress is positively homogeneous of degree one.

The Euler-Lagrange equations associated with (8) are consistent with a local equilibrium state for the microstructure with zero tractions on ∂H. In addition for the boundary condition 2) the Euler-Lagrange equations are associated with antiperiodic tractions on ∂V. In the case of boundary conditions 3) the stress boundary condition must be incorporated by means of a Lagrangian multiplier method based on the weak constraint (5), and the stationary point determines an equilibrium state of the micro-structure with zero tractions on ∂H and with homogeneous stress boundary conditions associated with the Lagrange parameter $\bar{\boldsymbol{\sigma}}$. Moreover for boundary conditions 2) and 3) the variational problem (8) gives the solution for $\boldsymbol{u}$ except for rigid body motions which can be excluded by adding appropriate artificial constraints.

As shown in [4], if the RVE is not statistically homogeneous, the following inequalities hold for strain fields corresponding to a common prescribed macro-strain $\bar{\boldsymbol{\varepsilon}}$ and RVE consisting of convex elastic constituents:

$$\bar{\boldsymbol{C}}^{(3)}\bar{\boldsymbol{\varepsilon}}\bullet\bar{\boldsymbol{\varepsilon}} \le \bar{\boldsymbol{C}}^{(2)}\bar{\boldsymbol{\varepsilon}}\bullet\bar{\boldsymbol{\varepsilon}} \le \bar{\boldsymbol{C}}^{(1)}\bar{\boldsymbol{\varepsilon}}\bullet\bar{\boldsymbol{\varepsilon}}, \tag{11}$$

where $\bar{\boldsymbol{C}}^{(i)}$ is the macroscopic moduli tensor corresponding to the i-th boundary condition in Eq. (5) evaluated with reference to a macro-strain direction.

2.2 Macroscopic constitutive properties

For a fixed damage configuration of the microstructure, the macroscopic constitutive law may be calculated by means of Eqs (9) and the resulting macroscopic stiffness tensor depends on the crack length l

$$\bar{\boldsymbol{\sigma}} = \bar{\boldsymbol{C}}(l)\bar{\boldsymbol{\varepsilon}}, \tag{12}$$

where in the presence of unilateral frictionless contact the macroscopic moduli tensor $\bar{\boldsymbol{C}}(l)$ may depend also on the direction of the prescribed strain, namely on the versor $\hat{\bar{\boldsymbol{\varepsilon}}} = \bar{\boldsymbol{\varepsilon}}/\|\bar{\boldsymbol{\varepsilon}}\|$.

Damage is assumed to be localized at the interface between micro-constituents or at crack surfaces, and the classical fracture mechanics criterion is used

$$G(\bar{\boldsymbol{\varepsilon}}, l) = G_c \quad then \quad \dot{l} \ge 0, \tag{13}$$

where G is the energy release rate associated with the crack length l and G_c is the fracture toughness of the material (see [21] for instance). From Eq. (13) it is possible to derive a non-linear damage evolution relation between the prescribed macro-strain and the crack length $l = l(\bar{\boldsymbol{\varepsilon}})$. As a consequence, the macroscopic stress-strain relation becomes highly non-linear and depends strongly on the macro-strain history.

The incremental constitutive relationship, taking into account for the evolutionary change in stiffness properties with progressive cracking, can be obtained by taking the derivative with respect to a time-like parameter t (l is a strictly increasing function of t) of Eq. (12):

$$\dot{\bar{\boldsymbol{\sigma}}} = \bar{\boldsymbol{D}}(\bar{\boldsymbol{\varepsilon}})\dot{\bar{\boldsymbol{\varepsilon}}}$$
$$\bar{\boldsymbol{D}}_{ijhk}(\bar{\boldsymbol{\varepsilon}}) = \bar{\boldsymbol{C}}_{ijhk}(l(\bar{\boldsymbol{\varepsilon}})) + \frac{d\bar{\boldsymbol{C}}_{ijmn}(l(\bar{\boldsymbol{\varepsilon}}))}{d\bar{\boldsymbol{\varepsilon}}_{hk}}\bar{\boldsymbol{\varepsilon}}_{mn}, \tag{14}$$

where a point denotes time derivative, and $\dot{l} > 0$ is assumed. If $\dot{l} \le 0$ the second term at the right hand side of $(14)_2$ vanishes. When approximate approaches are used to obtain effective stress-strain relations for the defected composite materials and damage evolution equations are available in closed form (see [14] for instance) then the second term at the right hand side of $((14)_2$ can be obtained by the chain rule of differentiation as $\left(d\bar{\boldsymbol{C}}_{ijmn}(l(\bar{\boldsymbol{\varepsilon}}))/dl\right)\left(dl/d\bar{\boldsymbol{\varepsilon}}_{hk}\right)$.

It is worth noting that while the tensor of macroscopic moduli $\bar{\boldsymbol{C}}(l)$ must be intended as a tangent moduli tensor with respect to the macro-strain when the damage configuration remains unchanged, the tensor

of incremental macroscopic moduli $\bar{\boldsymbol{D}}(\bar{\boldsymbol{\varepsilon}})$ is a tangent moduli tensor with respect to macro-strain when the fracture criterion is imposed.

3 Model description and numerical solution by FEM

When contact is excluded, the macroscopic moduli $\bar{\boldsymbol{C}}(l)$ are obtained, for a given damage configuration and a given microstructure, by using Eq. $(10)_2$ as:

$$\bar{C}_{ijhk}(l)=\frac{1}{|V|}\int_V C_{ijmn}(\boldsymbol{x})\,\varepsilon_{mn}(\boldsymbol{u}^{hk})\,dV\,. \tag{15}$$

Alternatively, the second expression in Eq. $(10)_2$ can also be used. For a prescribed macro-strain path $\beta\,\hat{\bar{\boldsymbol{\varepsilon}}}$, controlled by a parameter $\beta>0$ (serving as a load factor), the energy release rate for a given crack length is obtained by evaluating the *J*-integral along a closed contour enclosing the crack tip by post-processing the FEM equilibrium solution of the discretized microstructure. Due to linearity the energy release rate satisfies the following equation:

$$G\left(\beta\hat{\bar{\varepsilon}},l\right)=\beta^2 G\left(\hat{\bar{\varepsilon}},l\right), \tag{16}$$

therefore the damage evolution criterion (13) provides the critical load factor as

$$\beta=\sqrt{G_c/G\left(\hat{\bar{\varepsilon}},l\right)}, \tag{17}$$

and the moduli $\bar{\boldsymbol{C}}(l)$ can be obtained as functions of the macro-strain $\beta\,\hat{\bar{\boldsymbol{\varepsilon}}}$, when the fracture criterion is imposed.

When crack faces overlap the moduli ion Eq. (12) become dependent also on the macro-strain direction $\hat{\bar{\boldsymbol{\varepsilon}}}$. Therefore the moduli tensor $\bar{\boldsymbol{C}}\left(l,\hat{\bar{\boldsymbol{\varepsilon}}}\right)$ must be computed by means Eq. $(9)_2$ involving numerical determination. The macro-strain paths examined in the present work represent uniaxial extension/compression deformation modes in the x_1 and x_2 directions, namely $\hat{\bar{\boldsymbol{\varepsilon}}}_1^{\pm}=\pm\boldsymbol{e}_1\otimes\boldsymbol{e}_1$ and $\hat{\bar{\boldsymbol{\varepsilon}}}_2^{\pm}=\pm\boldsymbol{e}_2\otimes\boldsymbol{e}_2$, where the positive superscript refers to the extension direction whereas the negative one to the compressive direction.

It must be noted that moduli of kind $\bar{\boldsymbol{C}}\left[\hat{\bar{\boldsymbol{\varepsilon}}}_h\right]\bullet\boldsymbol{e}_i\otimes_s\boldsymbol{e}_j$, h=1,2, evaluated by computed as the *ij* macro-stress component (with the minus sign for the negative direction) corresponding to a positive or negative unit macrostrain $\hat{\bar{\boldsymbol{\varepsilon}}}_h$, according to the evidence that moduli are positively homogeneous of degree zero and depend only on the macro-strain path direction.

The non-linear macroscopic stress-strain relation (12) along the prescribed macro-strain path has been determined by calculating the macroscopic strain by Eq. (17) and the corresponding stress by Eq. $(2)_1$ as a function of the crack length, assuming a monotonic growth of damage. In order to simulate crack growth, an interface constitutive law has been used able to impose displacement continuity in the uncracked region and to impose unilateral frictionless contact in the cracked one. The interface constitutive law involves a stiffness parameter k dependent on the spatial coordinate, treated as penalty parameter:

$$\begin{aligned}&\boldsymbol{t}=\boldsymbol{k}(d)[\![\boldsymbol{u}]\!], && \boldsymbol{k}(d)=diag\{k_n,k_t\},\\ &\boldsymbol{t}=\{t_n,t_t\}, && [\![\boldsymbol{u}]\!]=\{[\![u_n]\!],[\![u_t]\!]\}\end{aligned}\quad, \tag{18}$$

$$k_t=\begin{cases}0 & d=1\\ k & d=0\end{cases},\ k_n=\begin{cases}\dfrac{k}{2}\left(1-sign[\![u_n]\!]\right) & d=1\\ k & d=0\end{cases}$$

where n and t denote normal and tangential directions to the interface, d is a crack parameter assuming the value 1 in the cracked region and 0 in the uncracked one, $\boldsymbol{t}$ is the traction vector acting on the positive side of the normal $\boldsymbol{n}$ to the interface, and $[\![\boldsymbol{u}]\!]$ is the displacement jump evaluated as the difference between the values from the negative and positive sides of the material interface. The penalty parameter assumes a value sufficiently large to ensure perfect adhesion but not too high to avoid numerical inaccuracy and unless otherwise stated in numerical computations the value kh=1e07E_m has been assumed, h being the side of the RVE. A continuation strategy is used by carrying out a parametric analysis with respect to k in which the nonlinear solver adopts the solution for the previous parameter value as initial guess.

It is worth noting that the use of fracture mechanics implies that crack initiation process is not taken into account and for l approaching to zero, an infinite value of the critical macro-strain should be attained, since energy release rate approaches to zero. Therefore the above macroscopic constitutive law has been computed with reference to a small initial relative crack length l_0/h, which in numerical applications has been chosen equal to 0.04 for the short fiber reinforced composite and equal to 0.0625 for the porous matrix material.

3.1 Computational implementation of the micro-to-macro transition

A displacement-type finite element approximation is adopted to discretize of the variational problem (7). The finite element model has been developed by using the commercial software COMSOL MULTIPHISYCS™ [20]. Appropriate artificial constraints are imposed in order to avoid rigid body motions of the RVE in the case of boundary conditions $(5)_2$ and $(5)_3$. In the case of boundary condition $(5)_2$, in order to exclude possible rigid body motions of the RVE, the fluctuation at the corner

points of the RVE are set to zero by means of constraints on point settings, implying that the corner points of the RVE are driven by the homogeneous deformation $\boldsymbol{u}(\boldsymbol{x}) = \bar{\boldsymbol{\varepsilon}}\boldsymbol{x}$.

The boundary conditions needed to apply the homogenization procedure have been imposed by means of point-wise constraints. The homogeneous fluctuation condition has been imposed by imposing the following boundary constraints:

$$\boldsymbol{u}(\boldsymbol{x}) = \bar{\boldsymbol{\varepsilon}}\boldsymbol{x} .$$

Periodic boundary conditions are imposed in the homogenization procedure making available the displacement field on the opposite boundary faces of the RVE, and are implemented by means of the extrusion coupling variable methodology [20].

Coupling variables are defined in two steps. First the source, namely the expression to evaluate and where to evaluate it, is defined; then the destination, that is, the domains within which you want to use the resulting variable, is defined. An extrusion coupling variable maps values from the source domain to the destination domain. Therefore since the domains are of the same space dimension, a point-wise mapping is obtained and the transformation between the source and destination is defined as a linear transformation.

Periodic boundary constraints are then imposed as constraints on the destination boundaries of the RVE, once the displacement is extruded as a coupling variable, by means of the following equation:

$$\boldsymbol{u}(\boldsymbol{x}^+) = \boldsymbol{u}^-(\boldsymbol{x}^-) + \bar{\boldsymbol{\varepsilon}}(\boldsymbol{x}^+ - \boldsymbol{x}^-) .$$

The homogeneous stress condition has been implemented by defining an integration coupling variables at some vertex in such a way that it represents the value of the integral at the right hand side of Eq. (4) to be constrained. The source of the coupling variable is the integral of the above expression over the RVE boundary. The destination of the integration coupling variable is a fictitious vertex. Then a point constraint is used to set the coupling variables to the desired *0* value. The uniform traction condition on the boundary of the RVE is imposed by using an integration coupling variables with global destination to compute the macro-stress nominal tensor according to Eq.$(1)_1$. Then the uniform traction condition $(5)_3$ is implemented as a weak constraint on the boundary of the RVE.

A computer code have been built in order to reproduce the non-linear constitutive law by using the COMSOL SCRIPT™ programming language which is interfaced with COMSOL MULTIPHISICS™. Crack growth is simulated by means of the non-linear interface constitutive law specified in Eq. (18), imposing displacement continuity across crack surfaces in the uncracked region and unilateral contact in the cracked one. The extension of the cracked region is enforced by assuming a discrete variation of the crack length with an increment equal to $\Delta l/h=0.01$.

The macroscopic quantities in Eqs (2) and (10) have been calculated by means of integration coupling variables. The source of the variable is the integral of the appropriate expression over the microstructure subdomains or boundaries. The destination of the integration coupling variable is the global destination, namely the integration coupling variables are available on all domains.

The homogenized moduli have been computed by means of numerical derivative using the central difference formula from the homogenized stress tensor:

$$\bar{C}_{ijhk}\left(\beta\hat{\bar{\boldsymbol{\varepsilon}}}, l\right) = \frac{\partial \bar{\sigma}_{ij}}{\partial \bar{\varepsilon}_{hk}}\left(\beta\hat{\bar{\boldsymbol{\varepsilon}}}, l\right) \simeq \frac{\bar{\sigma}_{ij}\left(\beta\hat{\bar{\boldsymbol{\varepsilon}}} + \boldsymbol{e}_h \otimes \boldsymbol{e}_k \Delta\bar{\varepsilon}_{hk}\right) - \bar{\sigma}_{ij}\left(\beta\hat{\bar{\boldsymbol{\varepsilon}}} - \boldsymbol{e}_h \otimes \boldsymbol{e}_k \Delta\bar{\varepsilon}_{hk}\right)}{2\Delta\bar{\varepsilon}_{hk}} .$$

3.2 *J*-integral evaluation

The energy release rate *G* for a given damage configuration and a prescribed macro-strain, is calculated by means of the *J*-integral technique ([18]). It has been proved rigorously that for a homogeneous hyperelastic body and a straight crack, *G* is equal to the value of the *J*-integral for any path enclosing the crack tip (see [19]). On the contrary for an inhomogeneous body, *G* is the limit value of the *J*-integral as the integration path approaches the crack tip.

In order to take advantage from the *J*-integral technique in the case of a micro-structure consisting of homogeneous hyperelastic constituents, it is necessary to carefully underline some assumptions regarding the integration path. The path-independence of the *J*-integral is a very attractive property as far as finite element analyses are used, since the integration path may be chosen sufficiently away from the crack tip where the description of the stress and strain field may be inaccurate due to the high gradient of the near-tip singular elastic field. In fact, numerical integration of singular terms contribute strongly to the loss of accuracy in the method. Therefore, to avoid integration of field quantities near the zone of dominance of the crack tip singularity, a path sufficiently away from the crack tip must be chosen. Studies on the relationship between the energy release rate and the *J*-integral and on the path independence of the *J*-integral for an heterogeneous body containing homogeneous micro-constituents, are lacking to the authors' knowledge. By application of the divergence theorem extended to region containing discontinuity lines (namely the micro-constituents material interfaces) and by the classical transport theorem, it can be proved that the energy release rate is equal to the limit value of the *J*-integral as the integration path approaches the crack tip also for the body containing

elastic inclusions, due to the traction continuity conditions at the interface between different constituents $[\![\boldsymbol{\sigma}]\!]\boldsymbol{n}=\boldsymbol{0}$. Therefore, the following relation holds for the energy release rate at a crack tip:

$$G(\bar{\boldsymbol{\varepsilon}},l)=\lim_{\delta\to 0}\boldsymbol{e}\bullet\int_{\partial D_\delta}\left(W\boldsymbol{n}-\nabla\boldsymbol{u}^T\boldsymbol{\sigma}\boldsymbol{n}\right)ds\,, \tag{19}$$

where D_δ is a disc of radius δ centered at the crack tip, $\boldsymbol{n}$ is the unit outward normal to ∂D_δ and $\boldsymbol{e}$ is the direction of crack propagation. Moreover, the path-independence of the *J*-integral can be proved for arbitrary paths Γ surrounding the crack tip which begin and end on the crack, individuating with ∂D_δ and the two faces of the crack a bounded region containing only material interfaces aligned with the direction of crack propagation $\boldsymbol{e}$:

$$G(\bar{\boldsymbol{\varepsilon}},l)=J(\Gamma,\bar{\boldsymbol{\varepsilon}},l)=\boldsymbol{e}\bullet\int_{\Gamma}\left(W\boldsymbol{n}-\nabla\boldsymbol{u}^T\boldsymbol{\sigma}\boldsymbol{n}\right)ds\,, \tag{20}$$

where $\boldsymbol{n}$ is the unit outward normal to Γ.

As a matter of fact, taking into account for material interfaces between micro-constituents in the application of the divergence theorem to the integral over the region *R* individuated by Γ, ∂D_δ and the two faces of the crack of the tensor field $W\boldsymbol{1}-\nabla\boldsymbol{u}^T\boldsymbol{\sigma}$, which is divergence free inside the regions occupied by the homogeneous micro-constituents, gives

$$\begin{aligned}\boldsymbol{e}\bullet\int_{\Gamma}\left(W\boldsymbol{n}-\nabla\boldsymbol{u}^T\boldsymbol{\sigma}\boldsymbol{n}\right)ds-\boldsymbol{e}\bullet\int_{\partial D_\delta}\left(W\boldsymbol{n}-\nabla\boldsymbol{u}^T\boldsymbol{\sigma}\boldsymbol{n}\right)ds+\\ \boldsymbol{e}\bullet\int_{\gamma}[\![W\boldsymbol{1}-\nabla\boldsymbol{u}^T\boldsymbol{\sigma}]\!]\boldsymbol{n}ds=0\end{aligned}\,, \tag{21}$$

where γ denotes the union of the material interfaces, $\boldsymbol{n}$ is the unit outward normal to ∂D_δ or Γ and the double brackets indicate the jump of the enclosed quantity evaluated as the difference between the values from the negative and positive sides of the material interface, namely:

$$[\![\boldsymbol{u}]\!]=\boldsymbol{u}^{-}-\boldsymbol{u}^{+}\,,$$

where $\boldsymbol{u}+$ ($\boldsymbol{u}-$) is the value of $\boldsymbol{u}$ immediately near the material interface at the positive (opposite) side of the normal $\boldsymbol{n}$ to the material interface. If the material interfaces are aligned with $\boldsymbol{e}$, the last term in Eq. (21), which can be rewritten as

$$\int_{\gamma}\left[[\![W\boldsymbol{1}]\!]\boldsymbol{n}\bullet\boldsymbol{e}-[\![(\nabla\boldsymbol{u}\,\boldsymbol{e})\bullet(\boldsymbol{\sigma}\boldsymbol{n})]\!]\right]ds\,, \tag{22}$$

vanishes since $\boldsymbol{n}$ and $\boldsymbol{e}$ are orthogonal and by noting that the directional derivative of $\boldsymbol{u}$ with respect to $\boldsymbol{e}$ is continuous across the material interface due to kinematical compatibility conditions (only discontinuities in the normal derivative $\partial\boldsymbol{u}/\partial\boldsymbol{n}$ are admitted for the displacement field across the material interface). As a consequence, Eq. (20) follows directly from Eq. (21). As it will be shown in the following the proved restricted path-independence of the *J*-integral is useful in view of applications to fiber reinforced composites.

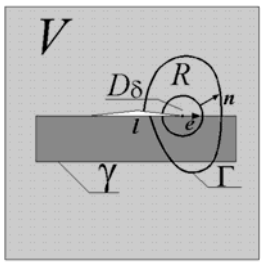

Fig. 2 Representation of contours leading to the path independence of the *J*-integral.

The *J*-integral evalution has been performed by using integration coupling variables [20] for post-processing purpose. The integration coupling variable has been defined as the integral expressed in Eq. (20) over the closed path Γ with a global destination.

4 Numerical determination of macroscopic constitutive laws of micro-structures

Two typical two-dimensional microstructures are considered as descriptive examples. The first one corresponds to a soft matrix containing a circular void. The side length of the RVE is denoted as *h*, and the diameter of the void is d=0.5h. The material constants are E_m=30GPa and ν_m=0.17. Micro-cracks of length l spread symmetrically from the void in the x_1 direction. In the second example a short fiber-reinforced composite is considered with a concentric fiber with diameter d_f and length l_f of, respectively, 0.05h and 0.5h, h being the side of the RVE. The material constants are E_m=2 GPa, ν_m=0.2, for the matrix, and E_f=30 E_m, ν_f=0.33, for the fiber. The fiber is perfectly bonded to the matrix except over a upper interface region of length l. Plane strain conditions are assumed.

The macroscopic moduli $\bar{\boldsymbol{C}}(l)$, and the macroscopic stress and strain quantities are independent on the size of the RVE provided that the crack length l is scaled with respect to the characteristic length of the RVE. On the contrary, when the fracture criterion is imposed the macroscopic stress and strain, obtained respectively by Eq. $(2)_1$ and by Eq. (16) as a function of the crack length, become dependent on the geometric and material properties of the RVE. As a matter of fact, it can be shown that for given Poisson ratios, a fixed ratio between E_f and E_m and given fiber volume fraction and fiber aspect ratio for the short fiber reinforced composite or void volume fraction for the porous matrix material, respectively, $G(\hat{\bar{\varepsilon}},l)$ is directly proportional with respect both to E_m and to a characteristic length of the RVE, denoted as l_c (the

side of the RVE h, the fiber length l_f or the void diameter d, for instance) and depends on the relative crack length l/h. As a consequence imposing the fracture criterion Eq. (17) shows that the dimensionless macro-strain $\beta\sqrt{E_m l_c / G_c}$ and the dimensionless macro-stress $\bar{\sigma}_{ij}\sqrt{l_c/(G_c E_m)}$ do not depend on the size of the RVE, on the matrix material longitudinal modulus and on the fracture toughness of the material or of the interface for the porous matrix material and the short fiber reinforced composite, respectively. Moreover the dimensionless energy release rate $G/(E_m l_c)$ will be used in order to avoid dependence on the size of the RVE and on the matrix material longitudinal modulus.

As shown in Fig. 3, both the microstructures are discretized by means of an unstructured mesh of quadratic triangular elements, with an appropriate mesh refinement along the contours used for the J-integral evaluation. Fig. 3 shows also the contours adopted to calculate the energy release rate at each crack tip. A typical mesh for the short fiber-reinforced composite is arranged in 26,294 triangular elements resulting in 106,376 degrees of freedom, whereas for the porous matrix material 35,680 elements are used giving 147,808 degrees of freedom.

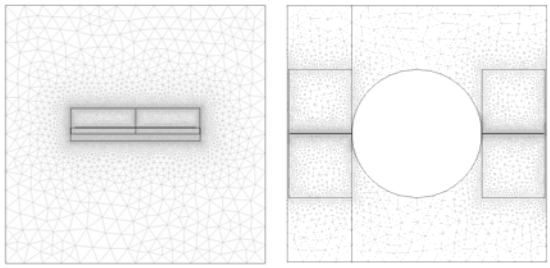

Fig. 3 Meshes of the porous matrix material (left) and of the short fiber reinforced composite (right), incorporating the paths used for the J-integral calculation.

Figs 4 and 5 depict the deformed configurations of the extension and compression uniaxial modes for the two considered micro-structures and the three boundary conditions used in the homogenization procedure: a) uniform tractions; b) periodic fluctuations and antiperiodic tractions.; c) linear displacements. For the sake of brevity a fixed damage configuration is considered characterized by relative crack lengths l/h=0.125 and l/h=0.24 for the porous matrix material and the short fiber reinforced composite, respectively.

From Fig. 4 it can be noted that for the positive directions of the uniaxial deformation modes $\hat{\hat{\boldsymbol{\varepsilon}}}_i^{+}$, i=1,2, crack faces do not overlap except for the uniform traction boundary condition and the extension deformation mode $\hat{\hat{\boldsymbol{\varepsilon}}}_1^{+}=\boldsymbol{e}_1\otimes\boldsymbol{e}_1$, where contact in a relatively small region near the void boundary occurs for relative crack lengths of about $0\le l/h\le 0.2$. The above contact region decreases as crack length increases and disappears for relative crack length l/h greater than 0.2. On the contrary, for negative directions of the uniaxial deformation modes $\hat{\hat{\boldsymbol{\varepsilon}}}_i^{-}$, i=1,2, crack faces always overlap, except for relatively small crack lengths for the deformation mode $\hat{\hat{\boldsymbol{\varepsilon}}}_1^{-}$ ($0\le l/h\le 0.07$) and uniform tractions boundary conditions. For the deformation mode $\hat{\hat{\boldsymbol{\varepsilon}}}_2^{-}$ crack is completely closed, whereas for $\hat{\hat{\boldsymbol{\varepsilon}}}_1^{-}$ and uniform traction boundary condition contact occurs only in a region near the crack tip (for instance when $l/h=0.125$ the region extends for a relative length of about 0.055).

In the case of the short fiber reinforced composite the situation is less variegated and from Fig. 5 observe that contact occurs for the macro-strain directions $\hat{\hat{\boldsymbol{\varepsilon}}}_1^{-}=-\boldsymbol{e}_1\otimes\boldsymbol{e}_1$, $\hat{\hat{\boldsymbol{\varepsilon}}}_2^{-}=-\boldsymbol{e}_2\otimes\boldsymbol{e}_2$ with the crack completely closed.

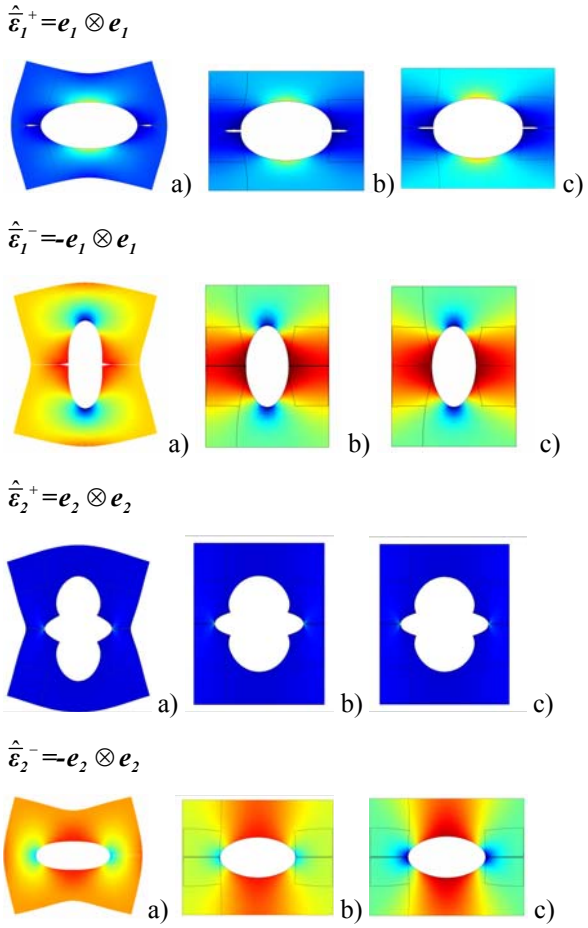

Fig. 4 Deformed configurations of the porous matrix material of the extension and compression uniaxial deformation modes, for different homogenization boundary conditions and for a relative crack length l/h=0.125.

$\hat{\bar{\varepsilon}}_1^{+}=\boldsymbol{e}_1\otimes\boldsymbol{e}_1$

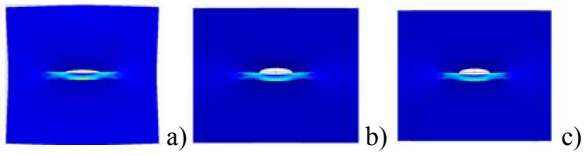

$\hat{\bar{\varepsilon}}_1^{-}=-\boldsymbol{e}_1\otimes\boldsymbol{e}_1$

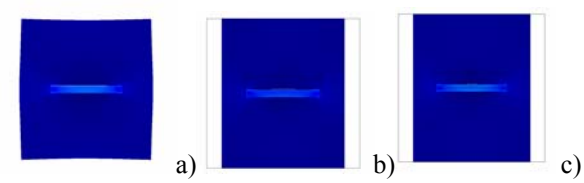

$\hat{\bar{\varepsilon}}_2^{+}=\boldsymbol{e}_2\otimes\boldsymbol{e}_2$

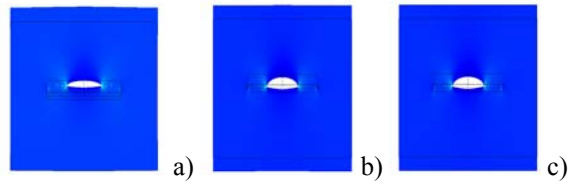

$\hat{\bar{\varepsilon}}_2^{-}=-\boldsymbol{e}_2\otimes\boldsymbol{e}_2$

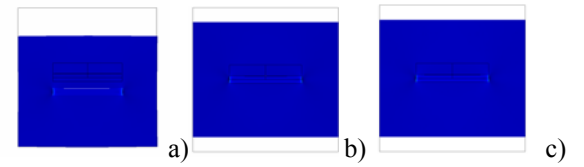

Fig. 5 Deformed configurations of the short fiber reinforced composite of the extension and compression uniaxial deformation modes, for different homogenization boundary conditions and for a relative crack length l/h=0.24.

4.1 Porous matrix material

The macroscopic stress-strain law for the uniaxial macro-strain paths along the x_1 direction is depicted in Figs 6a and 6b for the three boundary conditions used in the homogenization procedure: a) uniform tractions; b) periodic fluctuations and antiperiodic tractions; c) linear displacements. In the following figures E^* denotes $E_m/(1-\nu_m^2)$. For the sake of brevity only $\bar{\sigma}_{11}$ is shown. The initial linear behavior of the macroscopic constitutive law is characterized by the moduli $\bar{\boldsymbol{C}}(l_0)$ computed with reference to the initial crack length l_0. Numerical simulations have shown that for a extension mode $\hat{\bar{\varepsilon}}_1^{+}=\boldsymbol{e}_1\otimes\boldsymbol{e}_1$, contact occurs only for uniform tractions boundary conditions. In this case crack faces undergo contact in a small region near the void boundary for relative crack lengths of $0\le l/h\le 0.2$. In compression mode, $\hat{\bar{\varepsilon}}_1^{-}=-\boldsymbol{e}_1\otimes\boldsymbol{e}_1$, contact always takes place and crack is completely closed for linear and periodic boundary conditions whereas for uniform tractions condition contact occurs only in a region near the crack tip (for instance when $l/h=0.125$ the region extends for a relative length of about 0.055). The energy release rate is plotted in Figs 7a and b as a function of the relative crack length. As illustrated in Fig 7a, the energy release rate computed for the macro-strain direction $\hat{\bar{\varepsilon}}_1^{+}$, $G\left(\hat{\bar{\varepsilon}}_1^{+},l\right)$, is an increasing function of the crack length for the boundary conditions a) and b), whereas for c) a peak value is shown. The energy release rate is equal at both left and right crack tips.

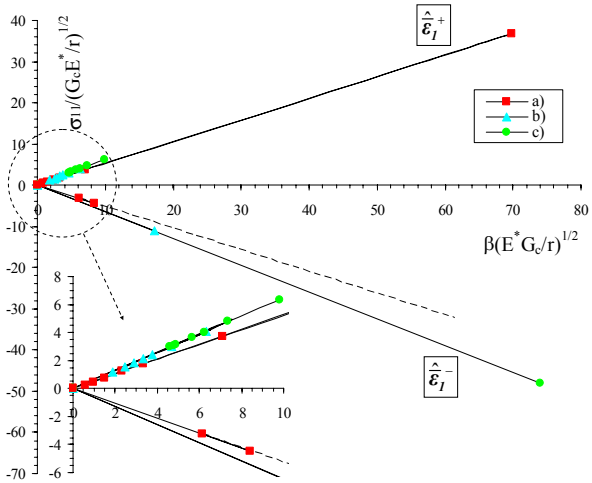

Fig. 6a Macroscopic dimensionless stress $\bar{\sigma}_{11}$ versus macroscopic strain for the macro-strain directions $\hat{\bar{\varepsilon}}_1^{\pm}$ and different homogenization boundary conditions.

With reference to the compression mode, Fig. 7b shows that the energy release rate $G\left(\hat{\bar{\varepsilon}}_1^{-},l\right)$ is practically independent on the crack length for periodic and linear deformations boundary conditions, whereas for uniform tractions boundary conditions the energy release rate shows a peak value and after reduces to zero for crack length greater than $0.06h$. As a consequence for the extension mode and boundary conditions a) and b) crack propagates at decreasing values of β and at fixed macro-strain crack propagates unstably. This causes a severe snap back in the macroscopic constitutive law. Except for very small crack lengths, for a prescribed macro-strain and in the case of the extension mode the energy release rate for periodic boundary conditions is bounded from below by that corresponding to linear deformations on the boundary and from above by that relative to uniform tractions. For the compression mode crack growth is neutral and the macroscopic constitutive law does not show the snap back for boundary conditions b) and c), whereas for boundary conditions a) a small snap back occurs with unloading accompanied by increase in crack length and after loading with no increase in crack length denoted by a dashed line.

Moduli are scarcely dependent on crack length especially for very small crack lengths, as it can be observed from Figs 8a and b, especially for the

ISBN 978-3-901608-32-2

compression mode. Consequently, the unloading branch of the macroscopic constitutive law is adjacent to the loading one. In the latter case moduli are practically a constant function of the crack length since crack is completely closed for all crack lengths for boundary conditions b) and c), whereas only partially for the one a). In the sake of brevity only the moduli $\bar{C}_{ij11}$ are shown.

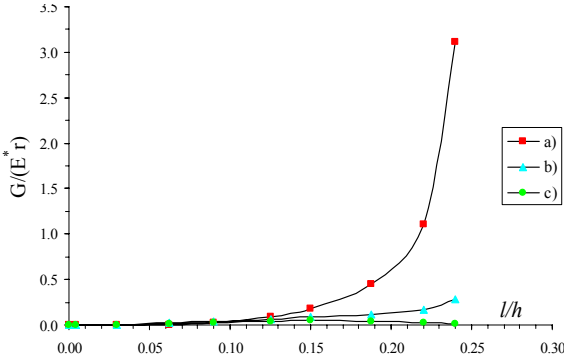

Fig. 7a Variation of the energy release rate as a function of crack length for the macro-strain path $\hat{\bar{\varepsilon}}_1^+$ and different homogenization boundary conditions.

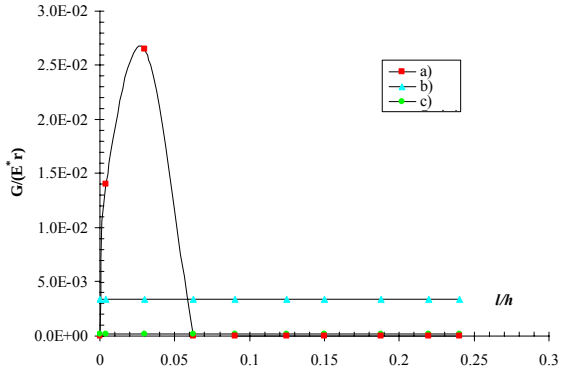

Fig. 7b Variation of the energy release rate as a function of crack length for the macro-strain path $\hat{\bar{\varepsilon}}_1^-$ and different homogenization boundary conditions.

According to Eq. (11) the modulus $\bar{C}_{1111}$ associated to periodic boundary conditions is bounded by those related to uniform tractions and linear deformations for every crack length. Moreover, observe in Figs 7 and 8 that both moduli and energy release rate are strongly dependent on the boundary conditions and, consequently, the macroscopic constitutive law is notably affected by the kind of boundary conditions imposed in the micro-to-macro transition. Macroscopic shear stress are absent for the three boundary conditions (5), within numerical errors related to the finite element discretization. Therefore, restricting the analysis to inplane macro-strain quantities, the macroscopic constitutive law has practically an orthotropic symmetry, since moduli $\bar{C}_{12jj}$ are practically zero. On the other hand, for $\hat{\bar{\varepsilon}}_1^-$ macroscopic moduli are practically independent on the crack length due to the strong influence of contact.

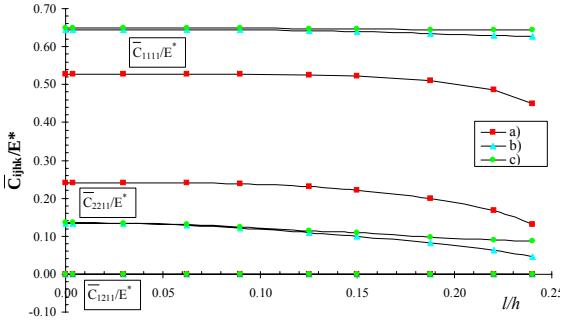

Fig. 8a Macroscopic moduli as functions of the crack length for the macro-strain direction $\hat{\bar{\varepsilon}}_1^+$ and different homogenization boundary conditions.

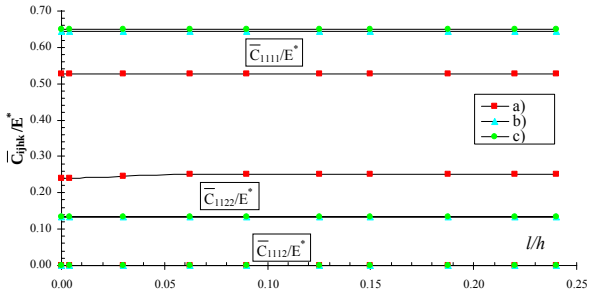

Fig. 8b Macroscopic moduli as functions of the crack length for the macro-strain direction $\hat{\bar{\varepsilon}}_1^-$ and different homogenization boundary conditions.

Fig. 9 illustrates the macroscopic stress-strain law for the uniaxial macro-strain paths along the x_2 direction for the three boundary conditions used in the homogenization procedure referred to as in the previous case. For the sake of brevity only $\bar{\sigma}_{22}$ is shown. Numerical simulations have shown that for a compression mode, $\hat{\bar{\varepsilon}}_2^- = -\boldsymbol{e}_2 \otimes \boldsymbol{e}_2$, contact takes place with the crack completely closed and the energy release rate becomes negligible. On the other hand crack faces do not overlap for $\hat{\bar{\varepsilon}}_2^+$. As a consequence in compression crack does not propagate, and the behavior in compression is linear elastic being characterized by the undamaged moduli $\bar{\boldsymbol{C}}\left(l = l_0\right)$ and it is denoted by a dashed line in Fig. 9.

As it can be noted by Fig. 10, the energy release rate, equal for both the left and right crack tips, for the macro-strain direction $G\left(\hat{\bar{\varepsilon}}_2^+, l\right)$ is a monotonic increasing function of the crack length only for periodic boundary conditions. For boundary conditions of linear deformations the energy release rate shows a peak value after which starts to decrease, whereas for uniform tractions boundary conditions it shows a maximum at about l/h=0.07 and, after, a minimum at about l/h=0.21. As a consequence crack propagates at decreasing values of β and at fixed

macro-strain crack propagates always unstably only for periodic boundary conditions, whereas for the boundary conditions a) and c) the possibility of crack arrest may occur. This causes a snap back in the macroscopic constitutive law in the case of periodic boundary conditions and snap-back and snap-through behaviors for the other two boundary conditions. For linear deformation boundary conditions the macroscopic constitutive law show a minimum after which macro-stress starts to increase. For relatively small crack lengths, namely $0 \le l/h \le 0.125$, for a prescribed macro-strain the energy release rate for periodic boundary conditions is bounded from below by that corresponding to linear deformations on the boundary and from above by that relative to uniform tractions.

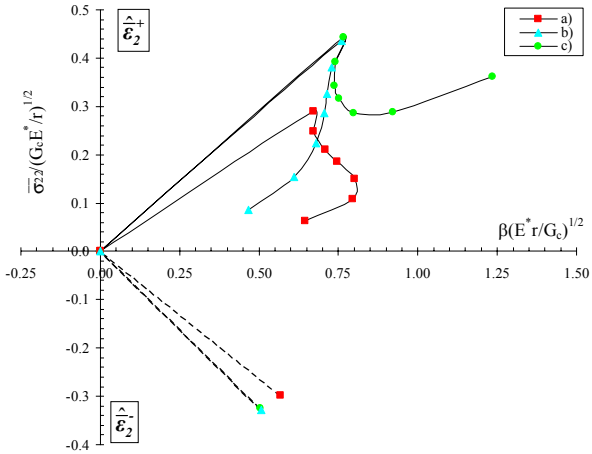

Fig. 9 Macroscopic dimensionless stress $\bar{\sigma}_{22}$ versus macroscopic strain for the macro-strain paths in the x_2 direction and different homogenization boundary conditions.

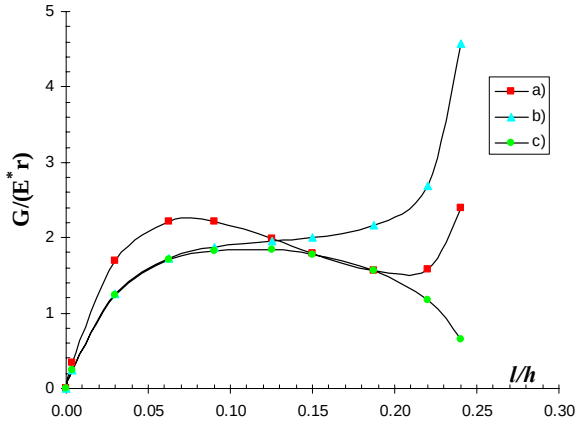

Fig. 10 Variation of the energy release rate as a function of crack length for the macro-strain direction $\hat{\bar{\varepsilon}}_2^+$ and different homogenization boundary conditions.

Moduli are strongly dependent on crack length especially for very large crack lengths, as it can be observed from Figs 11a and b. In addition they depend on the kind of boundary conditions although in the case of boundary conditions b) and c) the differences are very small. A large loss of stiffness is shown with respect to $\bar{C}_{2222}$. In the sake of brevity only the moduli $\bar{C}_{ij22}$ are shown. As already noted previously, the modulus $\bar{C}_{2222}$ associated to periodic boundary conditions is bounded by those related to uniform tractions and linear deformations. For $\hat{\bar{\boldsymbol{\varepsilon}}}_2^+ = \boldsymbol{e}_2 \otimes \boldsymbol{e}_2$, moreover, observe in Fig. 11a that both moduli and energy release rate are strongly dependent on the boundary conditions and, consequently, the macroscopic constitutive law is notably affected by the kind of boundary conditions imposed in the micro-to-macro transition. As already noted in the previous case, macroscopic shear stress are absent for the three boundary conditions (5), within numerical errors related to the finite element discretization, and the macroscopic constitutive law has practically an orthotropic symmetry. On the other hand, for $\hat{\bar{\boldsymbol{\varepsilon}}}_2^- = -\boldsymbol{e}_2 \otimes \boldsymbol{e}_2$ macroscopic moduli are practically independent on the crack length since crack is completely closed for every crack length.

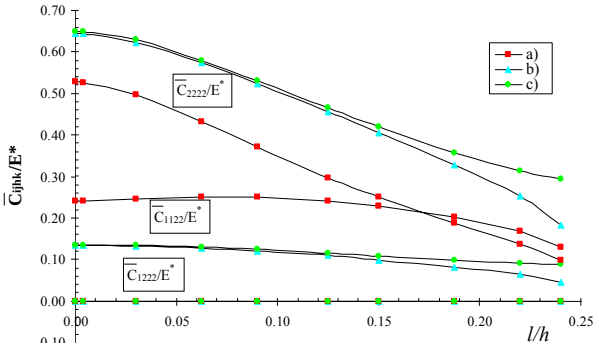

Fig. 11a Macroscopic moduli as functions of the crack length for the macro-strain direction $\hat{\bar{\varepsilon}}_2^+$ and different homogenization boundary conditions.

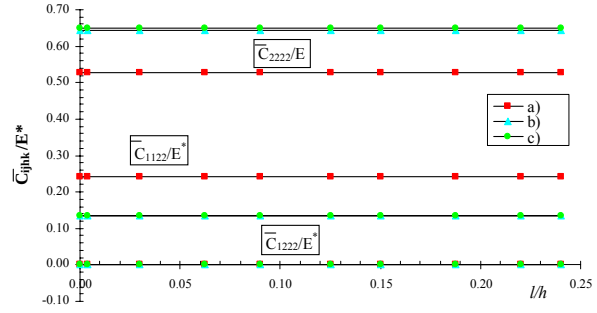

Fig. 11b Macroscopic moduli as functions of the crack length for the macro-strain direction $\hat{\bar{\varepsilon}}_2^-$ and different homogenization boundary conditions.

4.2 Short fiber reinforced composite

The macroscopic stress-strain law for the uniaxial extension and compression deformation modes along the x_1 direction is respectively depicted in Figs 12a and 12b for the three boundary conditions used in the homogenization procedure: a) uniform tractions; b) periodic fluctuations and antiperiodic tractions; c) linear displacements. As already noted before the initial linear behavior of the macroscopic constitutive law is characterized by the moduli $\bar{\boldsymbol{C}}(l_0)$ computed with reference to the initial crack length l_0. Numerical simulations have shown that for a compression mode, $\hat{\bar{\boldsymbol{\varepsilon}}}_1^- = -\boldsymbol{e}_1 \otimes \boldsymbol{e}_1$, contact takes place, therefore the macroscopic constitutive law show the expected dependence on the macro-strain path direction. On the contrary crack faces do not come in to contact for $\hat{\bar{\boldsymbol{\varepsilon}}}_1^+ = \boldsymbol{e}_1 \otimes \boldsymbol{e}_1$.

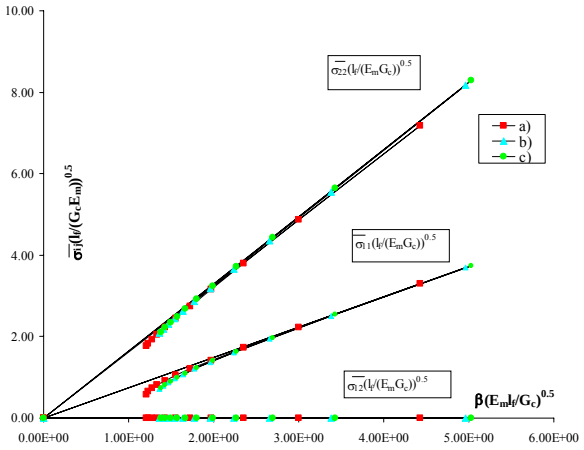

Fig. 12a Macroscopic dimensionless stresses versus macroscopic strain for the macro-strain direction $\hat{\bar{\boldsymbol{\varepsilon}}}_1^+$ and different homogenization boundary conditions.

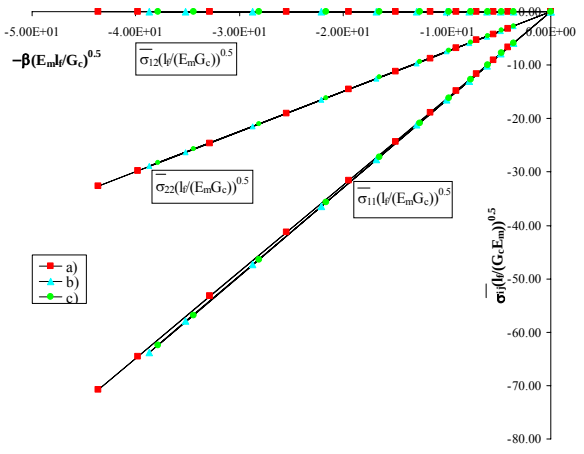

Fig. 12b Macroscopic dimensionless stresses versus macroscopic strain for the macro-strain direction $\hat{\bar{\boldsymbol{\varepsilon}}}_1^-$ and different homogenization boundary conditions.

The energy release rate, which is equal at both left and right crack tips, is plotted in Figs 13a and b as a function of the relative crack length. As illustrated in Figs 10, the energy release rate $G\left(\hat{\bar{\boldsymbol{\varepsilon}}}_1^{\mp}, l\right)$ is an increasing function of the crack length for all the boundary conditions and for both the extension and compression modes. As a consequence crack propagates at decreasing values of β and at fixed macro-strain crack propagates unstably. This causes a severe snap back in the macroscopic constitutive law. With reference to the extension (compression) mode, for a prescribed macro-strain the energy release rate for periodic boundary conditions is bounded from below by that corresponding to linear deformations (uniform tractions) on the boundary and from above by that relative to uniform tractions (linear deformations).

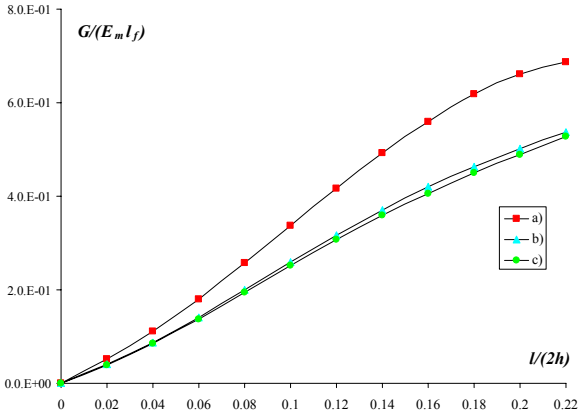

Fig. 13a Variation of the energy release rate as a function of crack length for the macro-strain direction $\hat{\bar{\boldsymbol{\varepsilon}}}_1^+$ and different homogenization boundary conditions.

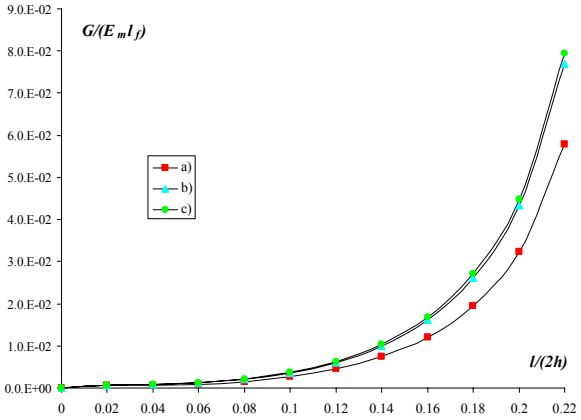

Fig. 13b Variation of the energy release rate as a function of crack length for the macro-strain direction $\hat{\bar{\boldsymbol{\varepsilon}}}_1^-$ and different homogenization boundary conditions.

In the case of the extension mode, moduli are scarcely dependent on crack length especially for very small crack lengths, whereas for the compression mode

moduli are practically independent on l due to contact effects, as it can be observed from Figs 14a and b. As a matter of fact, in the latter case moduli are practically a constant function of the crack length since crack is completely closed for all crack lengths. In the sake of brevity only the moduli $\bar{C}_{ij11}$ are shown. Moreover, observe in Figs 13 and 14 that both moduli and energy release rate are scarcely dependent on the boundary conditions especially for relatively small crack lengths and for boundary conditions b) and c), consequently, the macroscopic constitutive law is scarcely affected by the kind of boundary conditions imposed in the micro-to-macro transition. Macroscopic shear stress are practically absent for the three boundary conditions (5). Therefore, restricting the analysis to in-plane macro-strain quantities, the macroscopic constitutive law has practically an orthotropic symmetry, since moduli $\bar{C}_{12jj}$ are practically zero. The modulus $\bar{C}_{1111}$ associated to periodic boundary conditions is bounded by those related to uniform tractions and linear deformations.

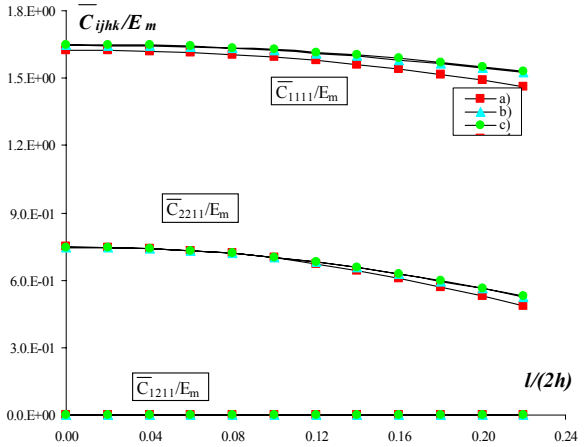

Fig. 14a Macroscopic moduli as functions of the crack length for the macro-strain direction $\hat{\bar{\varepsilon}}_1^+$ and different homogenization boundary conditions.

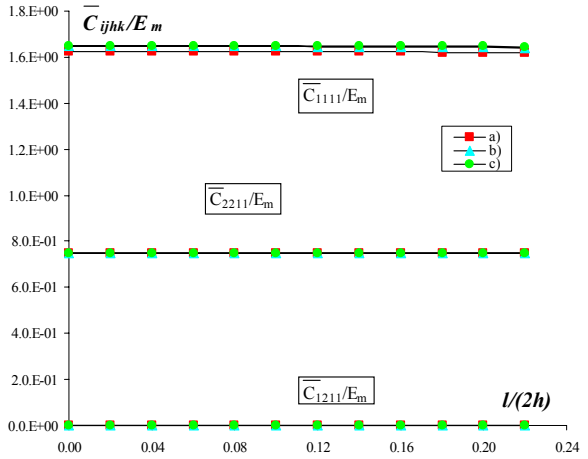

Fig. 14b Macroscopic moduli as functions of the crack length for the macro-strain direction $\hat{\bar{\varepsilon}}_1^-$ and different homogenization boundary conditions.

The macroscopic stress-strain law for the uniaxial deformation mode along the x_2 direction is depicted in Fig. 15 for the three boundary conditions used in the homogenization procedure. Numerical simulations have shown that for a compression mode, $\hat{\bar{\varepsilon}}_2^- = -\boldsymbol{e}_2 \otimes \boldsymbol{e}_2$, contact takes place with the crack completely closed and the energy release rate becomes negligible. On the other hand crack faces do not overlap for $\hat{\bar{\varepsilon}}_2^+$. As a consequence, in compression crack does not propagate, and the behavior in compression is linear elastic being characterized by the undamaged moduli $\bar{\boldsymbol{C}}(l = l_0)$ and it is denoted by a dashed line in Fig. 15. Moreover, as illustrated in Fig. 16, the energy release rate for the macro-strain direction $\hat{\bar{\varepsilon}}_2^+$, $G\left(\hat{\bar{\varepsilon}}_2^+, l\right)$, is an increasing function of the crack length for all the boundary conditions. The energy release rate shows equal values at both the left and right crack tips. As a consequence crack propagates at decreasing values of β and at fixed macro-strain crack propagates unstably. This causes a severe snap back in the macroscopic constitutive law. Except for very small crack lengths, for a prescribed macro-strain the energy release rate for periodic boundary conditions is bounded from below by that corresponding to linear deformations on the boundary and from above by that relative to uniform tractions.

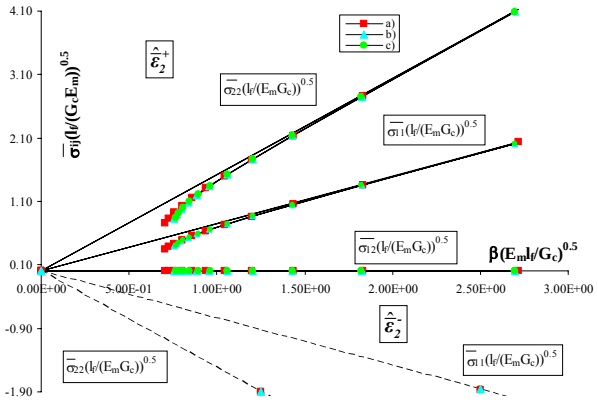

Fig. 15 Macroscopic dimensionless stresses versus macroscopic strain for the macro-strain paths in the x_2 direction and different homogenization boundary conditions.

As illustrated by Figs 17a and b, moduli are scarcely dependent on crack length especially for very small crack lengths and in the compression mode. In the sake of brevity only the moduli $\bar{C}_{ij22}$ are shown. For $\hat{\bar{\varepsilon}}_2^+$ moreover, observe in Figs 16 and 17a that both moduli and energy release rate are scarcely dependent on the boundary conditions especially for relatively small crack lengths and for boundary conditions b) and c), and, consequently, the macroscopic constitutive law is scarcely affected by the kind of boundary conditions imposed in the micro-to-macro transition. Similarly to the previous case macroscopic

shear stress are practically absent for the three boundary conditions (5), and the macroscopic constitutive law has practically an orthotropic symmetry. It is worth noting that, in line with Eq. (11) , the modulus $\overline{C}_{2222}$ associated to periodic boundary conditions is bounded by those related to uniform tractions and linear deformations.

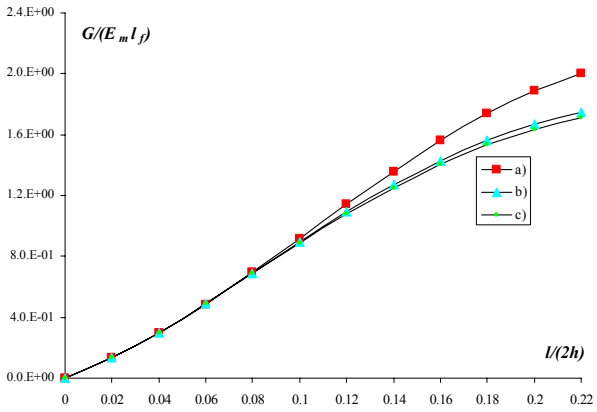

Fig. 16 Variation of the energy release rate as a function of crack length for the macro-strain path $\hat{\hat{\boldsymbol{\varepsilon}}}_2^+$ and different homogenization boundary conditions.

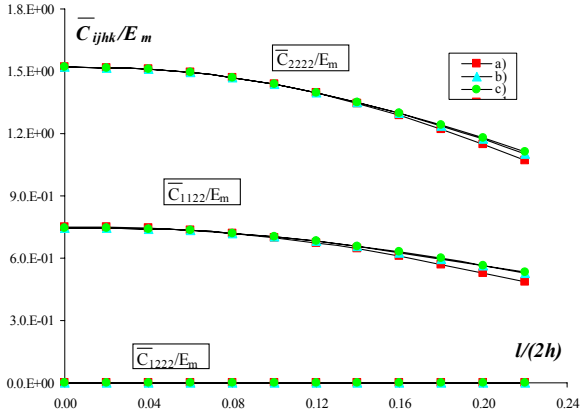

Fig. 17a Macroscopic moduli as functions of the crack length for the macro-strain path $\hat{\hat{\boldsymbol{\varepsilon}}}_2^+$ and different homogenization boundary conditions.

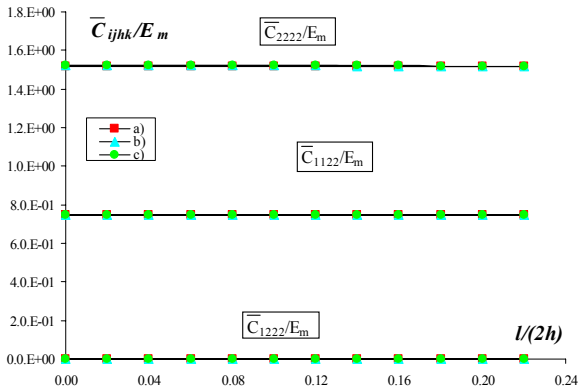

Fig. 17b Macroscopic moduli as functions of the crack length for the macro-strain path $\hat{\hat{\boldsymbol{\varepsilon}}}_2^-$ and different homogenization boundary conditions.

5 Conclusions

The influence of micro-cracking and crack faces contact on the effective properties of composite materials with heterogeneous micro-structure, is here investigated by means of the finite element method and interface models. When the changes in micro-structural configuration associated with the growth of micro-cracks and crack faces contact are taken into account, the macroscopic constitutive law turns out to be strongly non-linear. The non-linearity of the macroscopic constitutive law, often accompanied by severe snap backs and snap through, results in a progressive loss of stiffness which may lead to failure for homogeneous macro-deformations associated with unstable crack propagation. Damage evolution is simulated by micro-mechanical considerations using fracture mechanics. Both the cases of a brittle matrix composite containing micro-cavities with micro-cracks spreading from the cavity walls and of a fiber-reinforced composite with imperfect interfacial bonding are considered, loaded along extension and compression uniaxial macro-strain paths. The micro-structure is assumed to be controlled by the macroscopic deformation and three types of boundary conditions are studied, namely linear deformation, uniform tractions and periodic deformation and antiperiodic traction. Micro-crack propagation is modeled by using the *J*-integral methodology in conjunction with an interface model taking into account for contact between crack faces.

Results show the notable influence of damage and contact evolution, the type of boundary condition used to obtain effective properties in the context of macro-strain controlled microstructures and of the macro-deformation path, on the constitutive response of the homogenized material. In particular the effective properties of the porous matrix material are strongly dependent on the boundary conditions used in the micro-to macro transition. On the contrary, for the short-fiber reinforced composite the effective properties are scarcely affected by the boundary conditions, especially for small crack lengths. Moreover, generally speaking contact increases the macroscopic strength of the homogenized material by limiting the loss of stiffness. The proposed damage model is therefore able to give constitutive laws for the microstructure with evolving defects and to provide a failure model for a composite material undergoing micro-cracking and contact.

6 References

[1] J.C. Halpin, J.L. Kardos. The Halpin–Tsai equations: a review. *Polym Eng Sci*, 16:344–52, 1976.

[2] T. Mori, K. Tanaka. Average stress in matrix and average elastic energy of materials with misfitting inclusions. *Acta Metall*, 21:571–4, 1973.

[3] R. Hill. Elastic properties of reinforced solids: Some theoretical principles. *J Mech Phys Solids*, 11:357–72, 1963.

[4] S. Nemat-Nasser, M. Hori. Micromechanics: overall properties of heterogeneous materials. London. North-Holland. 1993.

[5] A. Benssousan, J.L. Lions, G. Papanicoulau. Asymptotic analysis for periodic structures. Amsterdam, North-Holland. 1978

[6] B. Hassani, E. Hinton. A review of homogenization and topology optimization I-homogenization theory for media with periodic structure. *Comput Struct*, 69:707–17, 1998.

[7] M. Hori, S. Nemat-Nasser. On two micromechanics theories for determining micro-macro relations in heterogeneous solids. *Mechanics of Materials*. 31:667±682, 1999.

[8] F.G. Yuan, N.J. Pagano, X. Cai. Elastic moduli of brittle matrix composites with interfacial debonding. *Int. J. Solids and Structures*, 34:177-201, 1997.

[9] P. Bisegna, R. Luciano, Bounds on the overall properties of composites with debonded frictionless interfaces, *Mech. Mater*, 28:23–32, 1998.

[10] S.F. Zheng, M. Denda, G.J. Weng. Interfacial partial debonding and its influence on the elasticity of a two-phase composite. *Mech Mater*, 32:695–709, 2000.

[11] H. Teng. Transverse stiffness properties of unidirectional fiber composites containing debonded fibers. *Composites: Part A*, 38:682–690, 2007.

[12] A. Caporale, R. Luciano, E. Sacco. Micromechanical analysis of interfacial debonding in unidirectional fiber-reinforced composites. *Computers & Structures*, 84:2200-2211, 2006.

[13] S. Li, Wang G., Morgan E. Effective elastic moduli of two dimensional solids with distributed cohesive microcracks. *European Journal of Mechanics A/Solids*, 23:925-933, 2004.

[14] S.A. Wimmer, D.G. Karr. Compressive failure of microcracked porous brittle solids. *Mechanics of materials,* 22:265-277, 1996.

[15] H. M. Jensen. Models of failure in compression of layered materials. *Mechanics of materials*, 3: 553-564, 1999.

[16] R. Hill, On constitutive macro-variables for heterogeneous solids at finite strain, *Proceedings of the Royal Society London, Series A,* 326:131–147, 1972.

[17] C. Miehe, Computational micro-to-macro transitions for discretized micro-structures of heterogeneous materials at finite strains based on the minimization of averaged incremental energy. *Comput. Methods Appl. Mech. Engrg*., 192: 559-591, 2003.

[18] J.R. Rice, A path independent integral in the approximate analysis of strain concentration by notches and cracks. *Journal of Applied Mechanics* Transactions of the ASME, 35: 379-386, 1968.

[19] M.E. Gurtin. On the energy release rate in quasi-static elastic crack propagation. *Journal of Elasticity*, 9: 187-195, 1979.

[20] COMSOL AB. COMSOL 3.2 Multiphysics User's Guide. September 2005.

[21] J.W. Hutchinson, Z. Suo. Mixed mode cracking in layered materials. Adv Appl Mech, 28. New York: Academic Press. 1992.